DOI: 10.1002/cphc.200800210

Visualization of Intrinsically Disordered Regions of Proteins by High-Speed Atomic Force Microscopy

Atsushi Miyagi,[a] Yasuo Tsunaka,[b, c] Takayuki Uchihashi,[a, d] Kouta Mayanagi,[b, e, f] Susumu Hirose,[g] Kosuke Morikawa,[b, d] and Toshio Ando*[a, d]

Intrinsically disordered (ID) regions of proteins are recognized to be involved in biological processes such as transcription, translation, and cellular signal transduction. Despite the important roles of ID regions, effective methods to observe these thin and flexible structures directly were not available. Herein, we use high-speed atomic force microscopy (AFM) to observe the heterodimeric FACT (facilitates chromatin transcription) protein, which is predicted to have large ID regions in each subunit. Successive AFM images of FACT on a mica surface, captured at rates of 5–17 frames per second, clearly reveal two distinct tail-like segments that protrude from the main body of FACT and fluctuate in position. Using deletion mutants of FACT, we identify these tail segments as the two major ID regions predicted from the amino acid sequences. Their mechanical properties estimated from the AFM images suggest that they have more relaxed structures than random coils. These observations demonstrate that this state-of-the-art microscopy method can be used to characterize unstructured protein segments that are difficult to visualize with other experimental techniques.

1. Introduction

Proteins encoded in eukaryotic genomes often contain unstructured regions (>50 residues).[1,2] These disordered regions lack intrinsically well-defined three-dimensional (3D) structures, but frequently fold into ordered conformations upon binding to their extrinsic targets; this folding is termed "coupled folding".[3] Such intrinsically disordered (ID) regions are highly conserved among species and are often involved in intra- and intermolecular recognition. Most unstructured segments comprise flexible linkers that play important roles in the assembly of macromolecular complexes and in the recognition of smaller biomolecules. The functional importance of ID regions was recently recognized, particularly in transcription, translation, and cellular signal transduction. However, the dynamics and functions of ID regions remain unclear at the molecular level. This is mainly due to a lack of useful techniques for analyzing unstructured segments of this sort at the single-molecule level. Indeed, X-ray crystallography and electron microscopy do not allow us to observe ID regions directly. Atomic force microscopy (AFM) is a widely used technique for imaging biological molecules at nanometer resolution.[4–6] The major advantage of AFM is that it can operate under physiological conditions, and it provides unique information by direct visualization of individual molecules in solutions. However, due to the poor temporal resolution of conventional AFM (about one frame per minute), only time-averaged features of proteins lacking large structural variation over time can be imaged. In solution, only samples that are firmly attached to a substrate directly or through adhesive chemicals can be observed; the alternative is to observe dried samples. Unfortunately, on drying, thin and flexible unstructured polypeptides tend to form lumps, or become flattened due to their strong attachment to a surface. In addition, they are not easily adsorbed onto substrate surfaces in solution, even with the assistance of adhesive chemicals. On the other hand, high-speed AFM, which can capture images at a rate surpassing ten frames per second, can directly visualize structural changes in biological molecules even against a background of Brownian motion.[7–10] Thus, high-speed AFM could potentially visualize unstructured ID regions of proteins.

Examples of typical ID regions have been identified in proteins constituting the complex machinery involved in transcrip-

[a] *A. Miyagi, Dr. T. Uchihashi, Prof. Dr. T. Ando*
Department of Physics
Kanazawa University
Kakuma-machi, Kanazawa 920-1192 (Japan)
Fax: (+81) 76-264-5739
E-mail: tando@kenroku.kanazawa-u.ac.jp

[b] *Dr. Y. Tsunaka, Dr. K. Mayanagi, Prof. Dr. K. Morikawa*
The Takara-Bio Endowed Laboratory
Institute for Protein Research, Osaka University
6-2-3 Furuedai, Suita, Osaka 565-0874 (Japan)

[c] *Dr. Y. Tsunaka*
JSPS, Ichiban-cho, Chiyoda-ku, Tokyo 102-8472 (Japan)

[d] *Dr. T. Uchihashi, Prof. Dr. K. Morikawa, Prof. Dr. T. Ando*
CREST, JST, Sanban-cho, Chiyoda-ku, Tokyo 102-0075 (Japan)

[e] *Dr. K. Mayanagi*
Nagahama Institute of Bio-Science and Technology
1266 Tamura-cho, NagahamaShiga 526-0829 (Japan)

[f] *Dr. K. Mayanagi*
BIRD, JST, 5-3 Yonban-cho, Chiyoda-ku, Tokyo 102-8666 (Japan)

[g] *Prof. Dr. S. Hirose*
Department of Development Genetics
National Institute of Genetics, Mishima
Shizuoka-ken 411-8540 (Japan)

Supporting information for this article is available on the WWW under http://dx.doi.org/10.1002/cphc.200800210.

tion.[11,12] For instance, the FACT (facilitates chromatin transcription) protein is predicted to contain large ID regions on the basis of its amino acid sequences. Displacement of histone H2A/H2B dimers from nucleosomes by FACT facilitates RNA polymerase II transcription[13,14] and chromatin remodeling.[15] FACT is highly conserved in eukaryotes, and is a heterodimer consisting of structure-specific recognition protein-1 (SSRP1) and SPT16; the latter has a higher molecular mass than the former. Intrinsically disordered regions are predicted to exist in the charge-enriched termini of SSRP1 and SPT16. The predicted ID region of SPT16 is essential for mRNA transcriptional elongation by FACT.[13] Herein, we use high-speed AFM to observe FACT and two of its deletion mutants. Successive AFM images, captured at an imaging rate exceeding five frames per second, clearly reveal two undulating tail-like structures of different lengths. The AFM analysis of the FACT deletion mutants demonstrates that the two tail domains correspond to the predicted ID regions of SSRP1 and SPT16. In addition, the analysis of the AFM images reveals a unique mechanical property of the tail domains that suggests more relaxed conformations than random coils.

2. Results and Discussion

2.1. Prediction of ID Regions in FACT

Primary-sequence analysis of FACT reveals that the smaller SSRP1 subunit contains a structure-specific recognition (SSRC) motif and a high-mobility group (HMG)-box domain, while SPT16 has an amino peptidase-like domain (WT in Figure 1). The solution structure of the *Drosophila* SSRP1-HMG-box domain was previously determined by NMR analysis.[16] Two C-terminal segments around the HMG domain (residues 405–554 and 625–723), indicated by red boxes in Figure 1, were predicted to be the ID regions of the SSRP1 subunit. The acidic C-terminal region (residues 889–1044) of the SPT16 subunit was also predicted to be an ID region, indicated by a blue box in Figure 1. Based on these predictions, we constructed two FACT mutants. The first FACT mutant, termed M1, includes an intact SPT16 subunit plus recombinant SSRP1 lacking 40% of the amino acids from the C terminus (M1 in Figure 1). The second FACT mutant, termed M2, includes an intact SSRP1 subunit plus SPT16 lacking 15% of the amino acids from the C terminus (M2 in Figure 1).

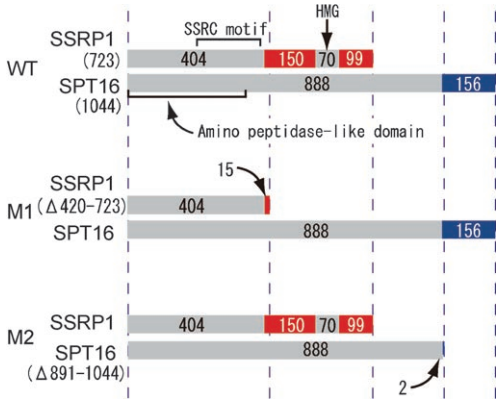

Figure 1. Schematic representation of the domain organization of the FACT proteins analyzed in this study. WT: Domain structure of wild type *Drosophila* SSRP1 and SPT16 proteins. The ID regions of SSRP1 and SPT 16 are predicted from their amino acid sequences and are highlighted in red (residues 405–554 and 625–723) for SSRP1 and blue (residues 889–1044) for SPT16. M1: Domain structure of the FACT mutant termed M1 in which SSRP1 residues 420–723 are deleted. Most of the SSRP1 ID regions, as well as the HMG domain, are missing. M2: Domain structure of the FACT mutant termed M2 that lacks the predicted SPT16 ID regions (residues 891–1044).

2.2. TEM Observation of Wild-Type FACT

We first obtained a TEM image of wild-type (WT) FACT (Figure 2). The TEM image shows particles of various sizes, most likely because FACT tends to form oligomers spontaneously. These oligomers were also indicated by gel filtration (data not shown). Currently, the physiological significance of FACT oligomerization is unclear. We observed that some particles have a minimum and similar size (arrows in Figure 2), which suggests that these particles correspond to the non-oligomerized (i.e., monomeric) FACT protein. The monomeric molecule is oval-shaped and about 15 nm in length along the major axis. The TEM images show solid and globular structures, but not tail-like structures.

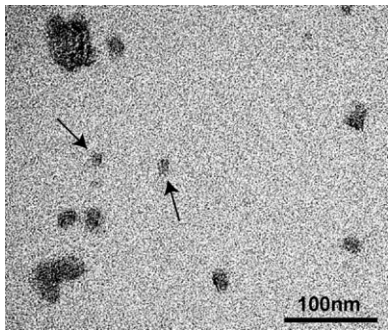

Figure 2. Transmission electron micrograph of FACT on a carbon-coated EM grid. Most of the FACT molecules form oligomers, but some remain monomers (indicated by arrows). The estimated size of the monomer is about 15 nm.

2.3. AFM Observation of WT FACT

High-speed AFM imaging also shows that WT FACT forms oligomers similar to those seen in the TEM images. We obtained successive AFM images of oligomeric FACT at an imaging rate of six frames per second (Figure 3 and Supporting Information, Video 1). Two distinct structures are clear in the images. The first one is a lumpy structure that appears to be strongly adsorbed onto the mica surface; its shape is almost unchanged over time. The second is a tail-like structure with a height of less than 1 nm. In the case of the oligomer shown in Figure 3, four tail-like structures are visible. We frequently detected several tail-like structures anchored to larger oligomers. These tail-like structures exhibit rapid fluctuations in position due to

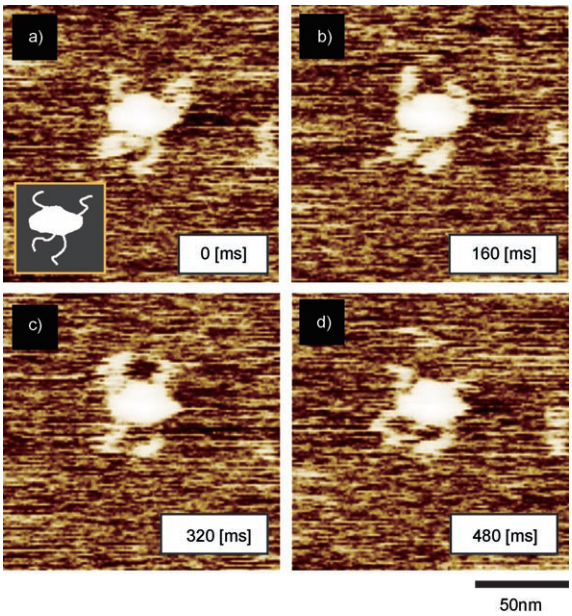

Figure 3. Successive AFM images of oligomerized FACT captured at an imaging rate of six frames per second. The scan range is 150×150 nm. A lumpy shape and four tail-like structures can be seen (see inset schematic). The position of the tail-like structures fluctuate markedly over time. The images were processed by using brightness-equalizing software.

Brownian motion, indicative of flexibility and relatively weak adsorption on the mica surface. We sometimes observed smaller particles with a globular shape and two tail-like structures of different lengths; an example is shown in Figure 4 and the Supporting Information (Video 2). In Figure 4a , the longer tail-like structure is labeled "i", and the shorter "ii". In the cross-section profile shown in Figure 4b , the height and full width of the major axis of the globular structure are about 4 and 25 nm, respectively. Taking into account the tip radius of about 4 nm, estimated with an electron microscope, the true width of the solid structure is approximately 17 nm.[17] This size is close to the size of a FACT monomer estimated from the TEM image. We therefore conclude that the image of the FACT protein shown in Figure 4 represents a monomer.

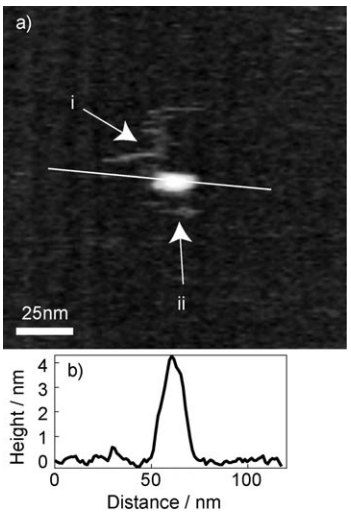

Figure 4. a) AFM image of a FACT monomer captured at an imaging rate of 6.4 frames per second. The scan size is 150×150 nm. One globular and two tail-like structures can be seen. The longer tail-like structure is indicated by 'i', and the other by "ii". b) Cross-sectional profile at the position indicated by the white line in a). The height and full width are about 4 and 25 nm, respectively. The size of the globular shape is consistent with that observed by TEM when the broadening effect of the tip radius is taken into account.

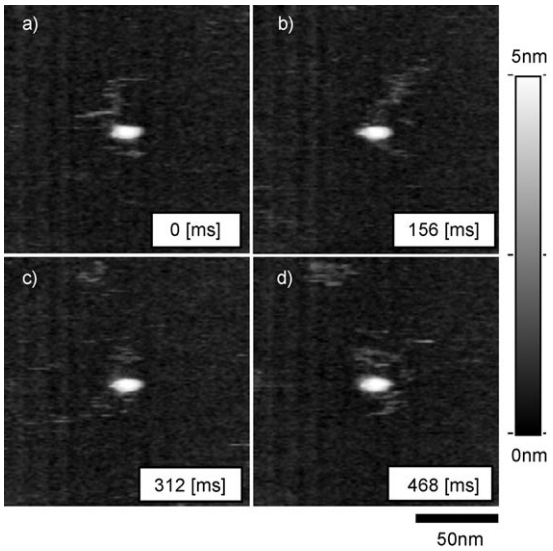

Figure 5. Successive AFM images of a FACT monomer taken every 156 ms. The scan size is 150×150 nm. The two tail domains appeared to wobble on the mica surface.

Figure 5 shows successive AFM images of a FACT monomer. This gallery of images clearly reveals the dynamic behavior of the two distinct tails that are anchored to the globular structure and undulate in the solution. Figure 6 shows a histogram

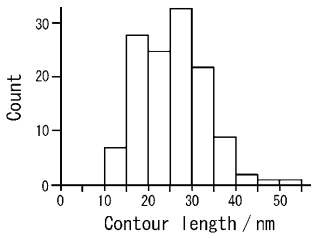

Figure 6. Histogram of the macroscopic contour length estimated for the tail domains. This shows two small peaks at 17.5 nm and 27.5 nm, although they are not statistically distinctive.

of the apparent contour lengths measured for the two tails. One can see two small peaks around 17.5 and 27.5 nm, although they are not so statistically distinctive. These observations suggest that the two observed tails correspond to the two large ID regions predicted from the amino acid sequences in both subunits (SSRP1 and STP16) of FACT. The estimated height of the tails is 0.6 nm. Slow AFM imaging of dried FACT samples do not show the tail structures (data not shown). This

is probably because these regions cannot remain extended under the conditions we used, or because the drying process flattens these regions so much that they are no longer detectable by AFM. In fact, under dried conditions, even the globular structure of FACT has a height of only about 0.6 nm (versus 4 nm by AFM in solution). Slow in-liquid imaging of FACT fixed on aminosilane- or spermine-coated surfaces also do not reveal the tail structures, and high-speed imaging of these samples shows that the ID regions are not firmly attached to the surfaces. Glutaraldehyde fixation of the samples on the aminosilane-treated surfaces results in lump-shaped structures that makes identification of the ID regions impossible. In addition, TEM combined with an averaging process cannot be applied because of the smeared images. We conclude that visualization of the thin unstructured ID regions of FACT is possible only by using high-speed AFM imaging in aqueous solutions.

2.4. Identification of the ID Regions of FACT by Means of Deletion Mutants

To determine definitively whether the predicted ID regions of FACT correspond to the tail structures observed with high-speed AFM, we constructed two FACT deletion mutants. In mutant M1, the predicted ID regions and the HMG-box domain of SSRP1 were deleted, and in M2 the predicted ID region of SPT16 was deleted. Representative high-speed AFM images of mutants M1 and M2 are shown in Figure 7 (also see

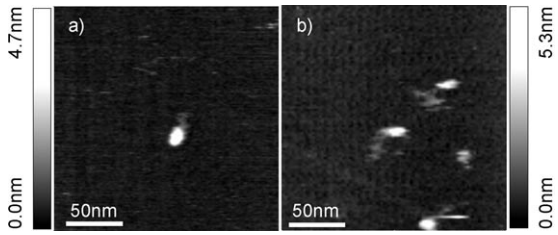

Figure 7. AFM images of the a) M1 and b) M2 mutants. The domain structures of the M1 and M2 mutants are depicted in Figure 1. Both images were acquired at an imaging rate of six frames per second. The scan range is 200×200 nm.

the Supporting Information, Video 3 and Video 4). The M1 mutant has only one short tail segment, as shown in Figure 7a, and the M2 mutant has only one longer tail segment. Therefore, the tail domains observed in the M1 and M2 mutants are assigned to the ID regions of SPT16 and SSRP1, respectively. The ID regions of SSRP1 and SPT16 contain 249 and 156 amino acid residues, respectively. It is thus reasonable that the tail structure observed in images of M2 is longer than that of M1. We measured the apparent contour lengths of both tails from the AFM images, and found that the averaged contour lengths of the observed tails of M1 and M2 are 17.8 and 26.2 nm, respectively (see histograms in Figure 8). In the most extended forms, the contours reach about 35 and 42 nm for the M1 and M2 tails, respectively. The wide distribution of apparent contour lengths is a fingerprint of the flexible structures. These average contour lengths approximately coincide with the two

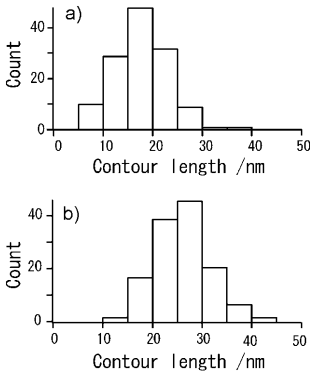

Figure 8. Histograms of the apparent contour lengths estimated for the tail segments of a) M1 and b) M2. The contour lengths at the peaks are 17.5 and 27.5 nm for M1 and M2, respectively, while their average values are 17.8 and 26.2 nm, respectively.

peak values of the histogram obtained for the WT-FACT shown in Figure 6. Assuming that the distance between two amino acid residues ranges from 0.15 to 0.36 nm, the stretched lengths of the predicted ID regions of SSRP1 and SPT16 are estimated to be 37–90 and 23–56 nm, respectively. The observed average lengths of the tails are approximately one-third of the theoretical maximum lengths. The observed maximum lengths are 50–60% of the theoretical maximum lengths. These differences are not due to an insufficient AFM imaging rate, as indicated in Section 2.5. Even for a completely loose polypeptide chain, its macroscopic contour length is shorter than the fully stretched length due to an entropic effect. For a polymer chain containing N identical segments which are connected through free joints, the entropic effect results in a smaller molecular size than the fully stretched form by a factor of $1/\sqrt{N}$.[18]

2.5. Imaging-Rate Dependence of ID Region Detection

We investigated the effect of the AFM imaging rate on the appearance of the tail-like structure in M2 (Figure 9). We used the M2 mutant for this study, since M2 has a longer ID region (i.e. a longer tail). At an imaging rate of 12.5 frames per second (Figure 9a), the tail-like ID region is clearly seen. Even at five frames per second (Figure 9b), the ID region is still observed as a string. However, the free end of the ID region seems broader in both these images, presumably due to its rapid changes in position. At two frames per second (Figure 9c), the ID region is still observable, but is blurry. Finally, at one frame per second (Figure 9d), the ID region is no longer discernible as a string, but appears hazy; even the ordered globular region of M2 has an irregular shape, probably because diffusion of M2 on the mica surface is faster than the imaging speed. These experiments suggest that an imaging rate greater than about five frames per second is required to visualize the ID regions of FACT clearly. Therefore, the imaging rate (six frames per second or higher) used for imaging M1 and M2 does not significantly affect the measurements of the apparent contour lengths of the ID regions.

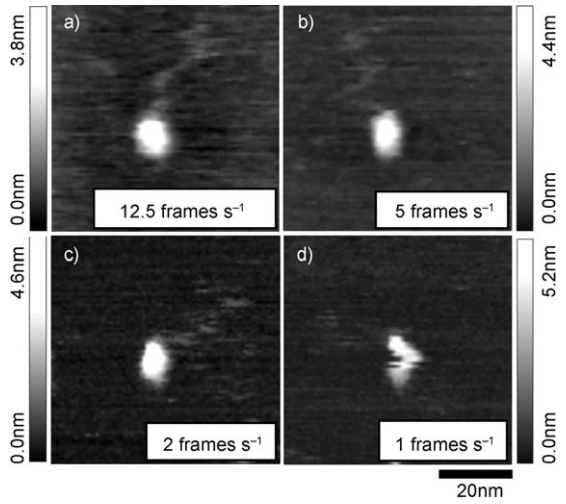

Figure 9. AFM images of mutant M2 acquired at different imaging rates. a) 12.5, b) 5, c) 2, and d) 1 frame per second. The images shown are 62×62 nm clipouts from 100×62 nm images obtained for the same single molecule of the M2 mutant.

2.6. Mechanical Properties of ID Regions

Here we analyze mechanical properties (stiffness and flexural relaxation time) of the observed tail-like structures. The stiffness of a polymer chain is described by the persistence length p of the chain, that is, the length over which the average correlation in the tangent direction decays by 1/e. In two dimensions, the mean square point-to-point distance of the chain is given by Equation (1)[19]

$$\langle r^2(l)\rangle_{2D} = 4pl\left[1 - \frac{2p}{l}\left(1 - e^{-l/2p}\right)\right] \quad (1)$$

where l is the contour length between two points on the chain. For $l\rightarrow\infty$, $\langle r^2(l)\rangle_{2D} = 4pl$. The persistence length depends on the hierarchy of the polymer structure. For example, the persistence length of a double-helical DNA strand is different from those of thicker strings formed by supercoiling of a DNA strand. In the AFM images obtained for the tail-like structures of FACT, polypeptide chains are not resolved. Therefore, the persistence lengths that can be obtained from the images are those for overall (macroscopic) string structures (see inset image in Figure 10b showing the relationship between the microscopic and macroscopic structures). We analyzed the tail-like structures of mutants M1 and M2. The mean-square point-to-point distance r^2 as a function of l is well-fitted by Equation (1) in both cases, and gives persistence lengths of 10.5 and 12.1 nm for the tail-likes structures of M1 and M2, respectively (Figure 10). These similar values indicate that the two ID regions have physically similar structures.

To estimate the persistence length of the microscopic structures of the ID regions, we assume that their C-terminal ends are located near the free ends of the tail-like structures. Under this assumption, the two-dimensional end-to-end distances R were obtained. The average distance $\langle R\rangle$ of the longer tail contained in M2 is 21.7 nm, while that of the shorter tail contained

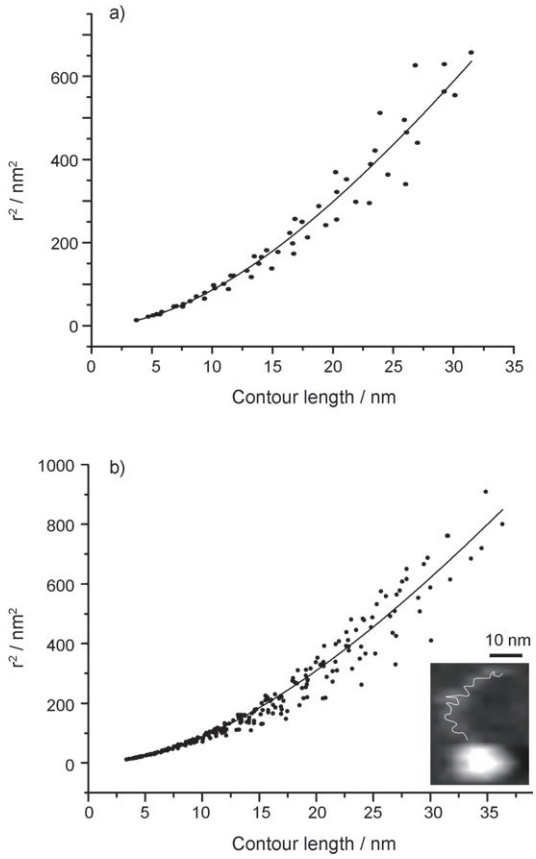

Figure 10. Persistence-length determination of the macroscopic structures of the tail segments of mutants a) M1 and b) M2. The mean-square point-to-point distance is plotted as a function of the macroscopic contour length between the corresponding two points. The solid lines indicate the best-fit curves of Equation (1) with a) $p = 10.5$ nm and b) $p = 12.1$ nm. The inset image indicates the relationship between the microscopic contour and the macroscopic structure. The microscopic contour is schematically drawn as a thin white line.

in M1 is 15.5 nm. The microscopic persistence lengths L_p were estimated by using these average values and the relationship $\langle R^2\rangle = 4L_pL$, where L is the polypeptide chain length. The ID regions and HMG-box domain of SSRP1 contain a total of 319 amino acid residues, while the ID region of SPT16 contains 156 amino acid residues. Supposing that the distance between adjacent amino acid residues is 0.36 nm for each adjacent couple, the microscopic contour lengths of the tail-like structures of M1 and M2 are 56 and 114 nm, respectively. Thus, the microscopic persistence lengths are estimated to be 1.2 and 1.1 nm for the tail-like structures of M1 and M2, respectively. The shorter persistence length of the M2 tail is likely due to the presence of the HMG-box domain. Note that these values are minimum estimates, since the employed values for the contour length are those at the maximum limit. Microscopic measurements of persistence length have previously been performed by measuring force–extension curves by AFM,[20,21] optical tweezers,[22] and magnetic tweezers.[23] The microscopic persistence length of the PEVK region (186 amino acid residues), which is responsible for the elastic property of titin and is thought to form a random coil, is reported to show a wide

range of L_p (0.4–2.5 nm, on average ca. 0.93 nm).[21] On the other hand, for proteins with ordered structures, the reported values for the microscopic persistence length are within a range of 0.36–0.5 nm.[20,24] Thus, the long microscopic persistence lengths of the ID regions of FACT are fingerprints of their very loose structures, which are slightly more relaxed than the random coil of the PEVK segment.

The Young modulus E is a material property that represents its stiffness and is related to the macroscopic persistence length by Equation (2)[25]

$$E = \frac{pk_BT}{H} \quad (2)$$

where k_B is the Boltzmann constant, T the absolute temperature, and H the momentum of inertia of the cross section of the object. Assuming that the tail-like structures of FACT are thin rods with radius ρ, H is given by $H=\pi\rho^4/4$. We estimated ρ (1–1.6 nm) from the width of the tail-like structures in several AFM images obtained by using different cantilever tips, taking into account the tip radii. The width is less affected by the substrate surface than the height, and its estimation is reliable when the sample height is similar to or smaller than the tip radius. Thus, the estimated Young modulus of the two tail-like structures is 9–58 MPa from their similar macroscopic persistence lengths. This estimated value of the macroscopic stiffness of the ID regions is 1–2 orders of magnitude smaller than those reported for globular proteins such as an actin monomer (ca. 2 GPa)[26] and lysozyme (0.5–2 GPa).[27,28] The value for an actin monomer was estimated from the force–extension relationship measured for single actin filaments.[26] The value of 0.5 GPa for lysozyme was estimated by AFM force–indentation experiments with a tip with a radius of about 20 nm,[27] and the value of 2 GPa for lysozyme by measuring the speed of ultrasound propagation through a lysozyme solution.[28] Therefore, these values represent the macroscopic stiffness of these proteins. Interestingly, the Young modulus as an estimate of the macroscopic stiffness of bovine carbonate anhydrase II is reported to be in the range of 2–6 MPa when the sample is incubated in the presence of 2–6 M guanidine·HCl.[29] Although these values of Young's modulus are somewhat smaller than those of the ID regions of FACT, the structures of the ID regions are considered to be roughly similar to those of denatured proteins.

A tethered polymer chain exhibits cyclic dynamics, and therefore its complex motion cannot be described simply with diffusion constants. Polymer dynamics is usually considered by using the Rouse model,[30] in which the polymer chain is modeled as a series of blobs (Rouse segments) connected by springs. The polymer motion contains a series of normal modes. However, in practical situations, the polymer dynamics is dominated by the slowest fundamental mode. In a small extension regime, the dynamics is similar in the longitudinal and transverse directions.[31] To estimate the relaxation time, we measured the end-to-end distance of the M2 tail as a function of time using images captured at 16.7 frames per second. Then, we calculated an autocorrelation function $G(\tau)=\langle R(t)-\langle R\rangle)\times[R(t+\tau)-\langle R\rangle]\rangle$. The autocorrelation function is nearly zero (data not shown), irrespective of the τ values (except for $\tau=0$), that is, the structural relaxation occurs faster than the imaging rate in spite of the presence of a drag effect of the mica surface.

2.7. Charged Residues in ID Regions

It was previously reported that a combination of low mean hydrophobicity and relatively high net charge is a prerequisite for the absence of ordered structures of proteins under physiological conditions.[32] In fact, the acidic and basic clusters are enriched in the ID regions of transcriptional factors and DNA binding proteins. These ID regions play important functional roles in transcriptional regulation.[33] The ID regions of FACT indeed have low hydrophobicity and both positively and negatively charged clusters (Figure 11). In our AFM observations,

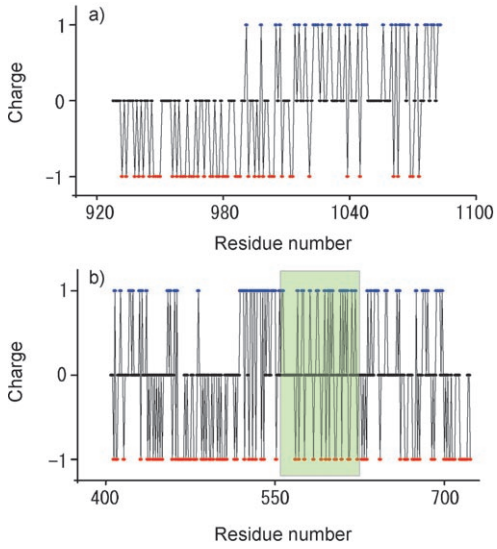

Figure 11. Distribution of charged amino acids in the ID regions of a) SPT16 and b) SSRP1. Positive and negative charges are indicated in blue and red, respectively. The HMG-box domain of SSRP1 is shaded green.

FACT and its mutants are placed on a negatively charged mica surface. In principle, it is possible that the electrostatic interaction between the basic clusters of FACT and the negative charges of a mica surface alter the native structures of the ID regions to form more extended forms. It is difficult to exclude this possibility, although we think that such alteration is unlikely, as the interaction is weak. However, the results are still interesting even were this to be the case, because DNA is also rich in negative charges and may act on FACT similarly to the mica surface.

3. Conclusion

This is the first study to use high-speed AFM to observe ID regions directly. The AFM images provide a direct view of FACT in solution on a mica surface; in this view, the two distinct tail-like structures of different lengths of FACT undulate and

wobble. This method for visualizing ID regions can be applied to other proteins, including mammalian nuclear proteins that contain many long unstructured segments. High-speed AFM can also be used to assist in successful protein crystallization, since predicted ID regions can be confirmed and deleted before crystallization to facilitate crystal growth. Herein, slow imaging of FACT samples that were dried or attached to a mica surface through adhesive chemicals did not reveal the tail structures. We found that imaging rates higher than about five frames per second are required to visualize the flexible ID regions clearly in physiological solutions. Our results indicate that high-speed AFM is a new imaging methodology that can be used to characterize flexible, unstructured segments of proteins at the single-molecule level.

Experimental Section

Prediction of ID Regions: ID regions of FACT were predicted by using the genomes-to-protein (GTOP) structures and functions database. The GTOP is a database of protein structures predicted from genome sequences.[34] Predictions were mainly carried out by using the homology search program PSI-BLAST.[35] Similar results were also predicted by other programs such as Disprot.[36]

Construction, Expression, and Purification of FACT Proteins: We used the same *Drosophila melanogaster* FACT cDNA as in our previous study.[15] The SSRP1 and SPT16 cDNAs were cloned into the pCold I and pCold III vectors, respectively.[37] The molecular masses of SSRP1 and SPT16 are 84 and 122 kDa, respectively. The expression plasmids were designed to co-express the SSRP1 and SPT16 proteins by using two inducible promoters in the pCold vectors.[38] The FACT proteins were simultaneously overexpressed in *Escherichia coli* strain BL21 (DE3). Protein co-expression was induced at $OD_{600} = 0.6$ by cold shock from 37 to 16 °C and by the addition of isopropyl-β-D-thiogalactopyranoside (IPTG, 1 mM). Cells were harvested, resuspended in buffer A containing Tris–HCl (20 mM) pH 8.5, NaCl (0.5 M), glycerol (10%), and 2-mercaptoethanol (5 mM), and lysed by sonication. After pelleting, the supernatant of the cell lysate was loaded onto a Histrap column (GE Healthcare). After washing the column with buffer A containing imidazole (20 mM), bound proteins were eluted with buffer A containing imidazole (500 mM). Finally, the proteins were purified on a Hitrap Q anion-exchange column (GE Healthcare) by elution with a concentration gradient of sodium chloride (0.25–1 M).

TEM Observations: To prepare specimens for TEM observation, an aliquot (3 μL) of a solution containing FACT was applied to each carbon-coated grid and negatively stained with uranyl acetate (2%). The specimens were examined with a JEM 1010 electron microscope (JEOL), operated at an accelerating voltage of 100 kV. Images were taken with a Bioscan CCD camera (GATAN). The step size of a pixel of the image was calibrated to be 5.1 Å by using TMV as a reference sample. A minimum-dose system (MDS) was used to reduce electron radiation damage to the sample.

High-Speed AFM Imaging: We used a laboratory-built high-speed AFM, details of which were described previously.[7,8] AFM images were acquired in tapping mode. We used cantilevers that were specially designed for high-speed imaging and provided by Olympus; the resonant frequency was about 1 MHz in water, and the spring constant was about 0.1 N m^{-1}. The quality factor of the cantilevers in water was about 2. As an AFM probe, we used an amorphous carbon tip grown on the cantilever by electron beam deposition. For high-speed AFM observation, a droplet (2 μL) of buffer A containing FACT (or the mutants M1 or M2) was deposited on a freshly cleaved mica surface. After incubation for 5 min, the sample was washed with buffer B, which contained Tris-HCl (20 mM) pH 7.5, $MgCl_2$ (10 mM), and KCl (50 mM). AFM observation was then performed under buffer B solution.

Slow AFM Imaging: AFM imaging of dried FACT samples was carried out in tapping mode at 0.004 frames per second on a Nanoscope IV (Veeco). The cantilevers with a thickness of 3.5–4.5 μm, a length of 115–135 μm, and a width of 30–40 μm were obtained from Veeco; the resonance frequency in air was 253–306 kHz, and the spring constant was 20–80 N m^{-1}. A drop (20 μL) of buffer A solution containing WT FACT was deposited on a freshly cleaved mica surface and incubated for 5 min. After washing the sample with buffer B and then with milli-Q water, the sample was dried with an air blower. FACT samples attached to modified mica surfaces in solution were imaged at 0.004 frames per second by using cantilevers (Bio-Lever mini, Olympus) with a thickness of 0.2 μm, a length of 37 μm, and a width of 16 μm; the resonance frequency was 25 kHz in water, and the spring constant was 0.1 N m^{-1}. Mica surfaces treated with aminosilane were prepared by placing a droplet (2 μL) of aminopropyltriethoxysilane (0.01 vol%) on a freshly cleaved mica surface for 5 min followed by washing with milli-Q water. For spermine-coated mica surfaces, a droplet (2 μL) of buffer B solution containing spermine (1 μg mL^{-1}) was used. For covalent attachment of FACT to a surface, the aminosilane-treated mica surface was further treated with a droplet (2 μL) of glutaraldehyde solution (0.01 vol%) for 5 min followed by rinsing with milli-Q water. Immediately after this treatment, FACT samples were placed on the prepared mica. However, glutaraldehyde activation resulted in surface roughness that was inappropriate for observing the tail structures of the FACT ID regions. In some cases, FACT samples placed on the aminosilane-treated mica surfaces were further treated with glutaraldehyde (0.01 vol%) for 5 min. The other procedures for slow AFM observation were the same as those for high-speed imaging, except that an imidazole buffer solution was used instead of Tris–HCl buffer.

Acknowledgements

This work was supported in part by the Core Research for Evolutional Science and Technology (CREST) of the Japan Science and Technology Agency (JST), by the Japan Society for the Promotion of Science (JSPS), by the Mitsubishi Foundation, and by a Grant-in-Aid for Basic Scientific Research (S) from MEXT Japan.

Keywords: atomic force microscopy · biophysics · protein modifications · protein structures · proteins

[1] A. K. Dunker, C. J. Brown, J. D. Lawson, L. M. Lakoucheva, Z. Obradovic, *Biochemistry* **2002**, *41*, 6573–6582.
[2] V. N. Uversky, *Protein Sci.* **2002**, *11*, 739–756.
[3] H. J. Dyson, P. E. Wright, *Nat. Rev. Mol. Cell Biol.* **2005**, *6*, 197–208.
[4] M. Radmacher, M. Fritz, H. G. Hansma, P. K. Hansma, *Science* **1994**, *265*, 1577–1579.
[5] H. Hansma, J. Hoh, *Annu. Rev. Biophys. Biomol. Struct.* **1994**, *23*, 115–139.
[6] D. J. Müller, H. Janovjak, T. Lehto, L. Kuershner, K. Anderson, *Prog. Biophys. Mol. Biol.* **2002**, *79*, 1–43.
[7] T. Ando, N. Kodera, E. Takai, D. Maruyama, K. Saito, A. Toda, *Proc. Natl. Acad. Sci. USA* **2001**, *98*, 12468–12472.
[8] T. Ando, T. Uchihashi, N. Kodera, A. Miyagi, R. Nakakita, H. Yamashita, M. Sakashita, *Jpn. J. Appl. Phys.* **2006**, *45*(3B), 1897–1903.

[9] T. Ando, N. Kodera, T. Uchihashi, A. Miyagi, R. Nakakita, H. Yamashita, K. Matada, *e.-J. Surf. Sci. Nanotech*. **2005**, *3*, 384–392.
[10] T. Ando, N. Kodera, Y. Naito, T. Kinoshita, K. Furuta, Y. Y. Toyoshima, *ChemPhysChem*. **2003**, *4*, 1196–1202.
[11] S. J. Demarest, M. Martinez-Yamout, J. Chung, H. Chen, W. Xu, H. J. Dyson, R. M. Evans, P. E. Wright, *Nature* **2002**, *415*, 549–553.
[12] Y. Minezaki, K. Homma, A. R. Kinjo, K. Nishikawa, *J. Mol. Biol.* **2006**, *359*, 1137–1149.
[13] R. Belotserkovskaya, S. Oh, V. A. Bondarenko, G. Orphanides, V. M. Studitsky, D. Reinberg, *Science* **2003**, *301*, 1090–1093.
[14] D. Reinberg, R. J. Sims III, *J. Biol. Chem.* **2006**, *281*, 23297–23301.
[15] T. Shimojima, M. Okada, T. Nakayama, H. Ueda, K. Okawa, A. Iwamatsu, H. Handa, S. Hirose, *Genes Dev.* **2003**, *17*, 1605–1616.
[16] N. Kasai, Y. Tsunaka, I. Ohki, S. Hirose, K. Morikawa, S. Tate, *J. Biomol. NMR* **2005**, *32*, 83–85.
[17] J. Vesenka, S. Manne, R. Giberson, T. Marsh, E. Henderson, *Biophys. J.* **1993**, *65*, 992–997.
[18] G. R. Strobl, *The Physics of Polymers*, Springer-Verlag, Berlin **1996**, pp. 23–50.
[19] C. Rivetti, M. Guthold, C. Bustamante, *J. Mol. Biol.* **1996**, *264*, 919–932.
[20] H. Dietz, M. Rief, *Proc. Natl. Acad. Sci. USA* **2004**, *101*, 16192–16197.
[21] H. Li, A. F. Oberhauser, S. D. Redick, M. Carrion-Vazquez, H. P. Erickson, J. M. Fernandez, *Proc. Natl. Acad. Sci. USA* **2001**, *98*, 10682–10686.
[22] S. B. Smith, Y. Cui, C. Bustamante, *Science* **1996**, *271*, 795–799.
[23] S. B. Smith, L. Finzi, C. Bustamante, *Science* **1992**, *258*, 1122–1126.
[24] D. J. Müller, W. Baumeister, A. Engel, *Proc. Natl. Acad. Sci. USA* **1999**, *96*, 13 170–13 174.
[25] G. S. Manning, *Biophys. J.* **2006**, *91*, 3607–3616.
[26] H. Kojima, A. Ishijima, T. Yanagida, *Proc. Natl. Acad. Sci. USA* **1994**, *91*, 12962–12966.
[27] M. Radmacher, M. Fritz, J. P. Cleveland, D. A. Walters, P. K. Hansma, *Langmuir* **1994**, *10*, 3809–3814.
[28] M. Tachibana, H. Koizumi, K. Kojima, *Phys. Rev. E* **2004**, *69*, 051921.
[29] R. Afrin, M. Alam, A. Ikai, *Protein. Sci.* **2005**, *14*, 1447–1457.
[30] P. Pincus, *Macromolecules* **1976**, *9*, 386–392.
[31] J. W. Hatfield, S. R. Quake, *Phys. Rev. Lett.* **1999**, *82*, 3548–3551.
[32] V. N. Uversky, J. R. Gillespie, A. L. Fink, *Proteins* **2000**, *41*, 415–427.
[33] S. Aizawa, H. Nishino, K. Saito, K. Kimura, H. Shirakawa, M. Yoshida, *Biochemistry* **1994**, *33*, 14690–14695.
[34] T. Kawabata, S. Fukuchi, K. Homma, M. Ota, J. Araki, T. Ito, N. Ichiyoshi, K. Nishikawa, *Nucleic Acids Res.* **2002**, *30*, 294–298.
[35] S. F. Altschul, T. L. Madden, A. A. Schaffer, J. Zhang, Z. Zhang, W. Miller, D. J. Lipman, *Nucleic Acids Res.* **1997**, *25*, 3389–3402.
[36] Z. Obradovic, K. Peng, S. Vucetic, P. Radivojac, C. J. Brown, A. K. Dunker, *Proteins* **2003**, *53*, 566–572.
[37] G. Qing, L. C. Ma, A. Khorchid, G. V. T. Swapna, T. K. Mal, M. M. Takayama, B. Xia, S. Phadtare, H. Ke, T. Acton, G. T. Montelione, M. Ikura, M. Inouye, *Nat. Biotechnol.* **2004**, *22*, 877–882.
[38] K. J. Kim, H. E. Kim, K. H. Lee, W. Han, M. J. Yi, J. Jeong, B. H. Oh, *Protein Sci.* **2004**, *13*, 1698–1703.

Received: April 7, 2008
Revised: July 4, 2008
Published online on August 12, 2008

